Elastic Properties of Cast Films from Propylene Elastomers

Andy H. Tsou,[1] Michael K. Lyon,[2] Bryan R. Chapman,[1] Sudhin Datta[2]

[1]*Corporate Strategic Research, ExxonMobil Research and Engineering Company, Annandale, New Jersey*
[2]*Baytown Technology & Engineering Complex-West, ExxonMobil Chemical Company, Baytown, Texas*

Received 16 April 2007; accepted 29 June 2007
DOI 10.1002/app.27184
Published online 10 October 2007 in Wiley InterScience (www.interscience.wiley.com).

ABSTRACT: Propylene-rich ethylene–propylene copolymers (P-E elastomers) made using metallocene catalysts exhibit excellent elastic properties, including high elongation to break and low tension set, particularly when blended with polyethylene or polypropylene and then compression molded. During film casting, the orientation imposed on a P-E elastomer lowers the extensibility and elastic recovery of films prepared from either neat P-E or P-E blends. A reduction in elongation to break of P-E films, with or without blending, was found to correlate with an increase in planar birefringence. The presence of dispersed phases of PP or high density polyethylene in P-E blends, which are drawn into elongated ellipsoids aligned in the machine direction, further reduces the recovery of these P-E blends. This reduction in elastic recovery for films made from P-E blends with aligned ellipsoidal dispersions was attributed to strain amplification around the dispersed particles in accordance with finite element simulation results, and was directly related to the dispersion tip radius. Films from P-E elastomer blended with high density polyethylene (high interfacial tension) were demonstrated to have lower planar orientation in addition to reduced dispersion deformation, and, therefore, better elastic properties, versus films in which the P-E elastomer was blended with PP (low interfacial tension). © 2007 Wiley Periodicals, Inc. J Appl Polym Sci 107: 1362–1372, 2008

Key words: elastic properties; cast films; propylene elastomer; metallocene; birefringence; interfacial tension; dispersion; finite element

INTRODUCTION

Propylene elastomers, hereinafter referred to as P-E elastomers, are commercially available semicrystalline, elastomeric copolymers composed predominantly of propylene with limited amounts of ethylene. An example of these products is Vistamaxx™ specialty elastomers from ExxonMobil, in which ethylene constitutes less than 20% of the total mass of each polymer chain. The placement of the propylene residues within the P-E elasomer chain is predominantly in a stereoregular isotactic manner leading to isotactic propylene crystallinity. The successful synthesis of these elastomers, which requires both intramolecular control of the tacticity of the inserted propylene units and intermolecular control of the composition of the polymer, is possible through the use of discrete metallocene catalysts. The combination of these catalysts with a solution polymerization process enables detailed control of the polymer characteristics, which define the properties of the polymer.

The presence of a limited amount of the isotactic propylene crystallinity renders the P-E elastomers as thermoplastic elastomers. The polypropylene crystalline domains in P-E elastomers act as network points (physical crosslinks) at room temperature. However, these junction points can be removed at higher temperatures to provide ease of processing for the material. The extent of crystallinity, which plays a critical role in determining the final physical properties, is attenuated by errors in the stereoregular placement of propylene monomers as well as by incorporation of ethylene in the chain backbone. These two sources of structural defects limit the average length of isotactic propylene runs, and consequently lower the crystalline content of the polymer. Typically, the heat of fusion is depressed to between 5 and 40 J/g. This range of crystallinity for P-E elastomers also sets bounds for both the elasticity and elastic recovery of these materials

In fact, the elastic behavior of P-E elastomers is complicated by their deformation-enhanced elasticity, wherein an initial deformation process brings about a lower set for subsequent extensions. Simultaneous measurements of the stress-strain behavior and the corresponding time-resolved synchrotron wide angle X-ray diffraction pattern for a P-E elastomer have revealed the molecular mechanism for deformation.[1] Initially, the crystalline lamellae are realigned along the stretching direction and simultaneously undergo a ''destruction'' process. At greater

Correspondence to: A. H. Tsou (andy.h.tsou@exxonmobil.com).

strains (i.e., in excess of 100%), strain-induced crystals with extended-chain conformation begin to form, and their number increases with continued deformation. After retraction many of these crystals remain, which enables the P-E to exhibit elastic behavior that is similar to that of a vulcanized natural rubber in subsequent extension and retraction cycles. In this case, the oriented crystals and nonoriented amorphous chain segments act as network points and flexible connectors between network points, respectively.

Because the elastic properties of P-E polymers arise predominantly from the amorphous chain segments, orientation caused by film processing is expected to impact the physical properties of the film. Maximum stretching (or elongation-to-break) of an amorphous polymer is known to be related to the stiffness of the chain segments between entanglements or network points.[2] Less flexible chain segments between permanent or temporary junction points typically results in a lower elongation-to-break. Induced orientation of the amorphous chain segments as a result of film processing reduces both the number of flexible segments and the entropy of the segments. This leads to lower elastic recovery. Additional deformation of the already oriented chains then has the effect of further lowering the entropy change, which further reduces the elastic recovery of a P-E cast film.

Cast films produced from low crystalline P-E elastomers are known to be difficult to handle owing to their soft and tacky nature. One way to address this problem is through addition of a fast-crystallizing immiscible polymer, such as iPP (isotactic polypropylene) or HDPE (high density polyethylene), which stiffens the material. However, the presence of such a ''hard'' dispersed phase is expected to have a significant impact on elastic properties of the resulting film. The extent of this effect depends on the mechanical properties of the dispersions, their size and shape distributions, as well as any orientation induced by the film fabrication process. The dispersion sizes, shapes, and orientation, in turn, are related to the interfacial tension and rheological properties of the blend components. In this study, the effect of the casting process on orientation and elastic properties of P-E cast films, including both neat P-E elastomer and its blends with moderate amounts of i-PP and HDPE, were investigated.

INTERFACIAL TENSION OF BLENDS

The conventional processes of measuring interfacial tension in polymer blends, such as the pendant drop method, the fiber retraction technique, or the breaking thread method, all demand optical contrast between the blend components. However, for molten polyolefin blends, this contrast is generally weak or nonexistent. The refractive indices of amorphous PP, amorphous PE, and P-E elastomer are 1.474, 1.48, and 1.48, respectively. This lack of optical contrast between P-E elastomer and its plastic PP or PE dispersions renders the conventional method inapplicable in determining their interfacial tensions.

Instead, in this study, small amplitude oscillatory shear (SAOS) experiments were conducted to measure the dynamic moduli of each blend and its neat components, while tapping phase atomic force microscopy (AFM) was used to determine the average size of the dispersed phase for the blend. The interfacial tension between the two blend components was then estimated by fitting the SAOS data to the Palierne model,[3] which describes the linear viscoelastic (i.e., small strain) behavior of a two-phase fluid containing viscoelastic spherical inclusions at a given dispersed phase concentration in a viscoelastic matrix.

The original derivation considered the dependence of interfacial tension on variations in surface area and resistance to shear to account for the presence of interfacial compatibilizers. Since the binary polyolefin blends evaluated in this study contain no interfacial modifiers, their complex moduli can be expressed by eq. (1),

$$G^*(\omega) = G_m^*(\omega)\left[\frac{1+\frac{3}{2}\phi_d\frac{E(\omega)}{D(\omega)}}{1-\phi_d\frac{E(\omega)}{D(\omega)}}\right] \tag{1}$$

In eq. (1), G* and G_m^* represent the complex moduli of the blend and matrix (continuous phase), respectively. The volume fraction of the inclusion (dispersed phase) ϕ_d, has a volume average radius R. The parameters $E(\omega)$ and $D(\omega)$ are calculated from G_m^*, the complex modulus of the dispersed phase G_d^*, and the interfacial tension between the two phases α, as follows:

$$E(\omega) = 2(G_d^* - G_m^*)(19G_d^* + 16G_m^*) + \frac{8\alpha}{R}(G_d^* + 2G_m^*) \tag{2a}$$

$$D(\omega) = (2G_d^* + 3G_m^*)(19G_d^* + 16G_m^*) + \frac{40\alpha}{R}(G_d^* + G_m^*). \tag{2b}$$

Setting $\alpha = 0$ in eq. (2) results in the linear viscoelastic extension of the Kerner equation for incompressible media.[4]

The dominant contribution to G^* from interfacial effects appears as an elastic contribution to the storage modulus (G') of the blend at low frequencies. Consequently, it is necessary to calculate G' and the

loss modulus (G'') for the blend from eq. (1). This requires taking the real and imaginary components of eq. (1), which can be expressed as a sum of products involving the loss modulus G_m'' and storage modulus G_m' of the matrix component,

$$G'(\omega) = AG_m'(\omega) - BG_m''(\omega) \tag{3a}$$

$$G''(\omega) = AG_m''(\omega) + BG_m'(\omega) \tag{3b}$$

In eqs. (3a) and (3b), the functions A and B can be expressed in terms of the in- (single quote superscript) and out-of-phase (double quote superscript) portions of $E(\omega)$ and $D(\omega)$,

$$A = \frac{\left[D'^2D''^2 + \frac{3\phi_d}{2}(E'D' + E''D'')\right]\left[D'^2D''^2 - \phi_d(E'D' + E''D'')\right] - \frac{3\phi_d{}^2}{2}(D'E'' - D''E')^2}{\left[D'^2 + D''^2 - \phi_d(E'D' + E''D'')\right]^2 + \phi_d^2(D'E'' - D''E')^2} \tag{4a}$$

$$B = \frac{\frac{5\phi_d}{2}[D'E'' - D''E']\left[D'^2 + D''^2\right]}{\left[D'^2 + D''^2 - \phi_d(E'D' + E''D'')\right]^2 + \phi_d^2(D'E'' - D''E')^2} \tag{4b}$$

These latter four functions D', E', D'', and E'' can then be expressed in terms of the measured storage and loss moduli for the two components of the blend,

$$D' = 38(G_d'^2 - G_d''^2) + 89(G_d'G_m' - G_d''G_m'') + 48(G_m'^2 - G_m''^2) + \frac{40\alpha}{R}(G_d' + G_m') \tag{5a}$$

$$D'' = 76(G_d' - G_d'') + 89(G_d'G_m'' + G_d''G_m') + 96G_m'G_m'' + \frac{40\alpha}{R}(G_d'' + G_m'') \tag{5b}$$

$$E' = 38(G'^2 - G_d''^2) - 6(G_m'G_d' + G_m''G_d'') - 32(G_m'^2 - G_m''^2) + \frac{8\alpha}{R}(5G_d' + 2G_m') \tag{5c}$$

$$E'' = 76(G_d'G_d'') - 6(G_m''G_d' + G_m'G_d'') - 64(G_m'G_m'') + \frac{8\alpha}{R}(5G_d'' + 2G_m'') \tag{5d}$$

Utilization of eqs. (3) to (5), in conjunction with small amplitude oscillatory shear data on both the blend and the neat components that constitute the blend, enables determination of α/R. Once the dispersion radius is known, the interfacial tension, α, can then be determined.

For a blend that contains a distribution of dispersion radii, it has been shown[5,6] that the volumetric mean radius can be used for the calculation of interfacial tension provided that the polydispersity index of dispersion radius does not exceed a value of two. The volume average radius of the dispersion was calculated by eq. (6),

$$R_v = \frac{\sum_{i=1}^{n} f_i R_i^4}{\sum_{i=1}^{n} f_i R_i^3} \tag{6}$$

Here f_i and R_i represent the number fraction and radius of the ith droplet, respectively. However, the AFM method used in this work yields a ''section size'' distribution of droplet sizes, as explained below, instead of the real three-dimensional size distribution. Therefore, a transformation from section size distributions to true particle size distributions was required before the computation of the volume average radius using eq. (6).

Particle or inclusion size distributions obtained from measurements in a thin section are a distorted version of the true distribution. When the overlap of images is negligible, the conversion of the observed distribution involves the solution of a Voterra integral equation of the second kind.[7] For the tapping-phase AFM method employed here to measure particle size, the depth of penetration into the sample is ~3 nm.[8] This section thickness is significantly less than the characteristic size of the dispersed phase for the blends of this study, which vary from 0.02 μm to several microns. Approximating the section thickness equal to zero, the Voterra integral equation is reduced to the solution attributed to Wicksell.[9] The integral equation that relates the distribution of apparent particle sizes, $g(x)$, to the true distribution of particle sizes, $f(x)$, is,

$$g(x) = \frac{x}{m}\int_x^X \frac{f(y)}{(y^2 - x^2)^{1/2}}\,dy \tag{7}$$

where m is the true mean diameter of the particles and X is the upper limit of the particle size. The function $f(x)$ is normalized to unity, i.e.,

$$\int_0^X f(x)\,dx = 1 \tag{8}$$

Although a closed form solution can be obtained for eq. (7), it requires numerical integration. In practice, a simple linear transformation of the frequencies in an observed histogram is applied. There are various analytical methods for determining size distributions of spheres from planar measurements.[10] The Schwartz-Saltykov method is based on measurements of section diameters. It is commonly applied for its simplicity, because it uses only one table of coefficients for any number of class intervals up to 15. Wicksell's solution for spherical particles is practically identical to that attributed to Schwartz-Saltykov. In the case of the latter analysis, the particle sizes can be broken down into any number of groups up to 15, depending on the accuracy required. In this study, all section sizes were separated into 15 groups. The general equation for the number of particles of any size group per unit volume, $(N_v)_i$, is given by,

$$(N_v)_j = \frac{k}{D_m}\sum_{i=j}^{k} a_i (N_A)_i \tag{9}$$

In eq. (9), $(N_A)_i$ is the number of particles of size i per unit area obtained from the micrograph, a_i are the coefficients for Schwartz-Saltykov method, which can be found elsewhere,[7] D_m is the largest diameter and k is the total number of groups.

EXPERIMENTAL

Materials and the cast film process

Compositions and molecular weights of P-E, PP, and high density polyethylene (HDPE) evaluated in this work are listed in Table I. Pelletized blends of P-E/PP or P-E/HDPE (80/20 weight ratio) along with 0.15 wt % hindered phenol (Irganox 1076) antioxidant were prepared using a Haake twin-screw extruder at 210°C. Portions of these blends were compression molded into 1.8 mm thick pads at 150 to 180°C for 3 to 5 min, and allowed to age for 14 days before mechanical testing. Cast films from these blends were manufactured by chill-roll casting using a 10-cm tape die on the same Haake extruder at 210°C and two extrusion rates: 40 RPM and 80 RPM. Cast films from neat P-E extruded at 40 RPM were aged for 14 days at room temperature before mechanical property testing; the film thickness ranged from 0.11 to 0.22 mm for these samples. Portions of both sets of films were subsequently annealed in an oven for 1 min at 70°C, which exceeds the melting temperature of the P-E but is less than the melting temperatures of PE and iPP, to relax P-E orientation. Mechanical properties for these annealed samples were also measured.

TABLE I
Compositions and Molecular Weights of P-E, PP, and HDPE

Material	Composition	M_n	M_w	M_z
P-E	P-E	96,000	174,000	266,000
PP4292	iPP	72,000	222,000	407,000
PD4443	iPP	51,000	153,000	259,000
HD7755	HDPE	5300	197,000	770,000
HD6705	HDPE	16,000	56,000	135,000

Interfacial tension

All blends investigated were 80/20 blends by weight so that the volume fraction of the dispersion is low to minimize the spatial overlap of the dispersed droplets. Overlapping effects can introduce errors in dispersion counting and sizing.[11] Rheological experiments were performed on a DSR500 (Rheometric Scientific) stress rheometer utilizing the 25 mm diameter cone (0.1 rad cone angle) and plate geometry. Four to five decades of frequency were applied to each sample from the highest frequency of 500 rad/s to the lowest of 10^{-2} rad/s at 210°C. To maintain the applied strain at a constant value at each frequency that was probed, the prescribed stress was reduced 37% each time the frequency was reduced to its next value. To acquire an observable secondary plateau at low frequencies, i.e., less than 1 rad/s, from the interfacial stress, the storage moduli of the blend at low frequencies were required to have a value that is less than 1000 Pa at the test temperature. Subsequent to characterizing the dynamic behavior of each blend and its neat components, the blend data were fitted to calculated results from the Palierne model. This last step determined a best-fit for the ratio of the interfacial tension to the average dispersed phase droplet radius.

Following rheological testing, each polymer blend test specimen was cooled and carefully removed from the rheometer with minimal deformation, and subjected to AFM analysis. A minimum of five different areas was examined by tapping-phase AFM per sample surface after cyrofacing. Image sizes varied from 2 μm × 2 μm to 40 × 40 μm, so that spatial and magnification biases were minimized. The images were processed and contrast enhanced using PHOTOSHOP™ (Adobe Systems, San Jose, CA). After thresholding, section size distributions of the dispersion in each blend were measured using an image processing tool kit (Reindeer Games, Rayleigh, NC). True size dispersed phase particle size distributions were then calculated from the planar measure-

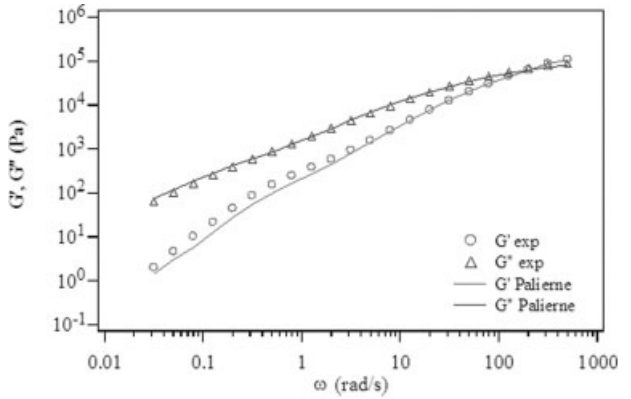

Figure 1 Rheological data for the P-E/HD6705 blend. The solid lines are a best fit to the data calculated using the Palierne model.

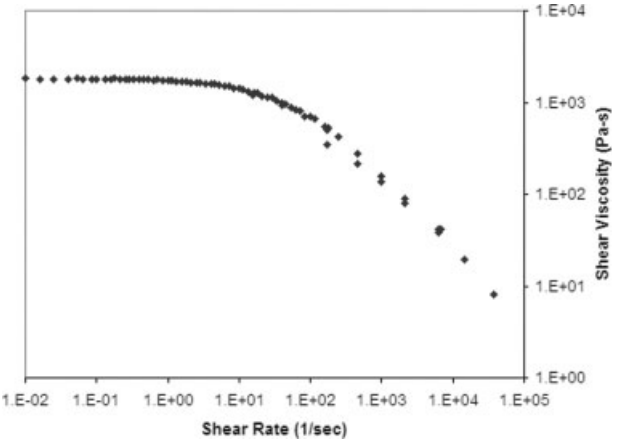

Figure 2 Flow curve of P-E.

ments using the Schwartz-Saltykov method with 15 class intervals. In turn, a volume average diameter was determined for each blend from its measured true size distributions and the interfacial tension was calculated.

For all the immiscible blends, a secondary plateau appeared for G' at low frequencies exemplified by the blend of P-E/HD6705 (see Fig. 1). By finding the best fit to the dynamic measurements with calculated volume average diameters from tapping phase AFM micrographs, interfacial tensions for all the blends evaluated were determined by the Palierne method and are listed in Table II. Although P-E is more compatible with PP than PE, the interfacial tensions between P-E and PP are in fact comparable with that between P-E and the lower molecular weight HDPE (HD6705). This reflects the strong effect of molecular weight on interfacial tension. The value of 1.3 mN/m between P-E and PP4292 is in general agreement with the value obtained using Small Angle Neutron Scattering (SANS) at 210°C.

Shear viscosity

Flow curves at 210°C (see Figs. 2–4) for the five polymers listed in Table II were generated from data acquired on a Rosand capillary rheometer, combined with the small amplitude oscillatory shear data described earlier. For each polymer the empirical Cox-Merz rule was found to be applicable for equating the complex viscosity determined via SAOS testing to the Bagley and Rabinowitsch corrected capillary data. This resulted in the acquisition of data that encompassed eight decades of shear rate. Zero shear viscosities extracted from these measurements are listed in Table III. Despite large differences in zero-shear viscosity, these polymers exhibited similar shear thinning behavior and consequently, similar viscosity values at high shear rates (i.e., shear rate greater than 100 rad/s).

TABLE II
Interfacial Tensions in P-E/PP and P-E/HDPE Blends

Blends	Interfacial tension (mN/m)
P-E/PP4292	1.3
P-E/PD4443	0.02
P-E/HD7755	8.5
P-E/HD6705	0.7

Optical birefringence

Refractive indices of P-E films were measured using the Metricon 2001 (Metricon). The measurement area was a circle of 1-mm diameter with index resolution of 0.0003–0.0005. The operating wavelength was 632.8 nm generated by a low-power He-Ne laser. Samples were brought into contact with the base of a prism by means of a pneumatically operated coupling head. No contact fluids were applied. Two birefringence values are calculated in these mechani-

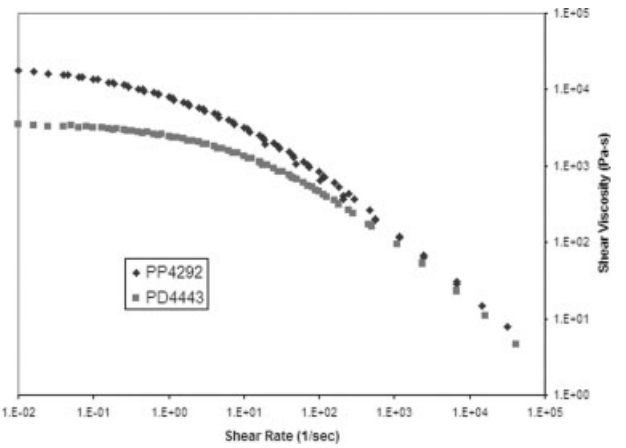

Figure 3 Flow curves of PP4292 and PD4443.

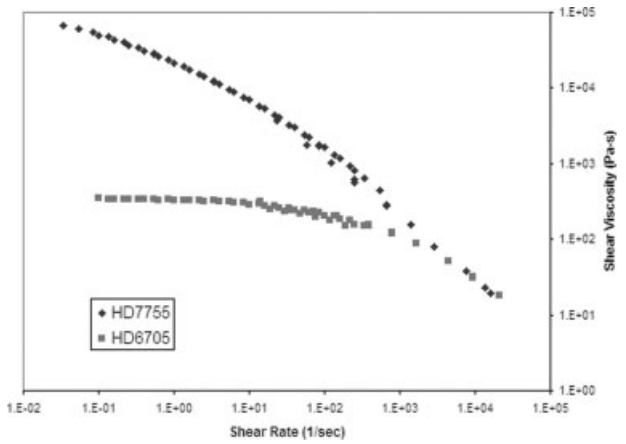

Figure 4 Flow curves of HD7755 and HD6705.

cally orthotropic films to express relative orientation. One is the in-plane birefringence, IBR, which measures the relative in-plane orientation with respect to the machine direction (MD):

$$\mathrm{IBR} = n_1 - n_2 \tag{10}$$

where n is the refractive index and subscripts 1, 2, and 3 refer to machine, transverse, and normal directions, respectively. The other is the planar birefringence, PBR, which measures the orientation with respect to the film plane normal (ND). Samuels and coworkers[12] referred the PBR as the planarity index.

$$\mathrm{PBR} = (n_1 + n_2)/2 - n_3 \tag{11}$$

The average refractive index in an anisotropic film is defined as

$$\langle \mathrm{n} \rangle = (n1 + n2 + n3)/3 \tag{12}$$

This average refractive index is the same as the refractive index of an optically isotropic polymer film of the same density. The average refractive index is related to the density of the film and is proportional to its degree of crystallinity.

Atomic force microscopy

For AFM morphology analysis, all films were cyrofaced at −150°C in a Reichert cryogenic microtome using a diamond knife in both MD-ND and TD-ND directions (MD, TD, and ND represent machine, transverse, and normal directions for a film, respectively). To prevent moisture condensation onto the sample surface while warming them to room temperature, the samples were stored in a nitrogen-purged desicator immediately after cryofacing. The faced samples were then mounted in a miniature vise for AFM analysis. Tapping phase AFM analyses were performed using a Digital Instrument Dimension 3000 instrument, which was operated under ambient conditions. A FESP tip with a resonant frequency of 60–70 kHz was used.

Tapping phase contrast arises from variations in mechanical properties between the phases in the presence of conservative and dissipative tip-sample interactions.[13] To minimize the adhesion-energy-loss contribution to phase contrast (or to emphasize the mechanical contribution to phase contrast), hard tapping with a set amplitude that was less than or equal to 50% of the initial amplitude was applied. AFM phase images of all specimens were converted into a TIFF format and processed using PHOTOSHOP™ (Adobe Systems). An image processing tool kit (Reindeer Games) was applied for image measurements. Results were written into a text file for subsequent data processing using EXCEL™ (Microsoft Corp., Seattle, WA) for computing the size and shape of the dispersed phase.

Mechanical properties and finite element simulation

Tensile mechanical testing was done using an Instron (Instron) tester at a crosshead travel rate of 5 in/min for tensile properties and at a rate of 20 in/min for elastic recovery and set. All data are reported in engineering stress and strain terms. Tension sets were determined from the residual lengths of blend samples instantaneously after relaxing from 100% extension.

COSMOS/M™ finite element code (Structural Research and Analysis Corp., Santa Monica, CA) was applied to simulate the deformation behavior of a two-dimensional plane-stress P-E containing a single PP or HDPE dispersion. A spherical dispersion and a 4/1 elliptical dispersion of the same area were evaluated. The area coverage of the dispersion in P-E was 3%. Both P-E and its dispersion were assumed to be linear elastic with the properties listed in Table IV. Elastic moduli were estimated based on experimentally determined 100% moduli. Plane 2D quadrilateral elements with 8 nodes per elements were used. Nonlinear analysis was performed with updated

TABLE III
Zero Shear Viscosities of P-E, PP, and HDPE Evaluated

Polymer	Zero shear viscosity (210°C, Pa s)
P-E	1900
PP4292	18,000
PD4443	3200
HD7755	100,000
HD6705	340

TABLE IV
Mechanical Properties of P-E, PP, and HDPE Used for Finite Element Simulation

Material	Modulus (psi)	Poisson's ratio	Specific gravity
P-E	500	0.49	0.86
PP	150,000	0.41	0.91
PE	80,000	0.49	0.96

Lagrangian formulation based on an Almansi strain tensor and a Cauchy stress tensor using a Newton-Raphson integration scheme. The boundary condition was imposed by displacement control.

RESULTS AND DISCUSSIONS

Morphology of P-E films

AFM tapping phase micrographs of the MD-ND plane of cast films of P-E/PP and P-E/PE extruded at 40 RPM are shown in Figures 5–8. Large variations in aspect ratios and sizes of these ellipsoidal dispersions as a function of the dispersion type are indicated. The long axis of all dispersions is aligned in the machine direction. Dispersion morphologies in these films in the TD-ND plane are of similar ellipsoidal shape but with lower aspect ratios. A representative morphology from P-E/PP4292 cast film is shown in Figure 9. The long axes of these ellipses in TD-ND plane are parallel to the transverse direction.

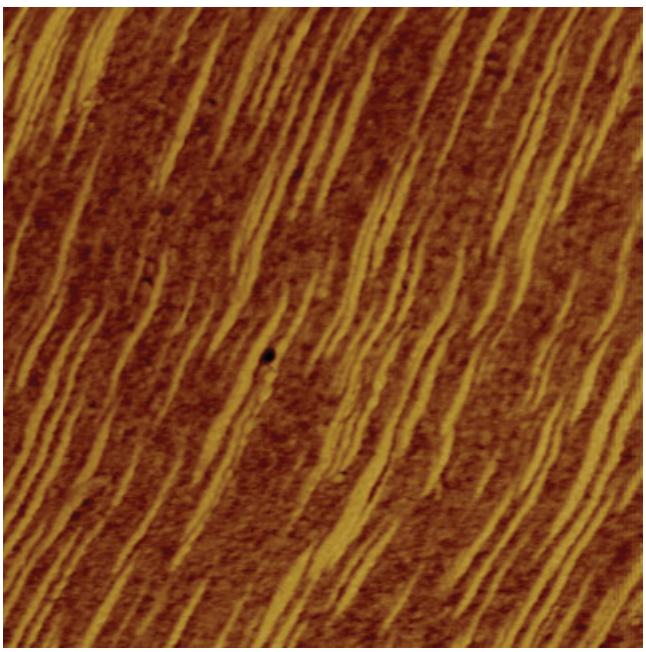

Figure 6 AFM tapping phase micrograph of P-E/PD4443 cast film in MD-ND plane (5 μm by 5 μm). [Color figure can be viewed in the online issue, which is available at www.interscience.wiley.com.]

Image processing provided dimensions of these ellipsoidal dispersions (see Table V). Large variations in aspect ratios and sizes of these ellipsoidal dispersions as a function of the dispersion type are indi-

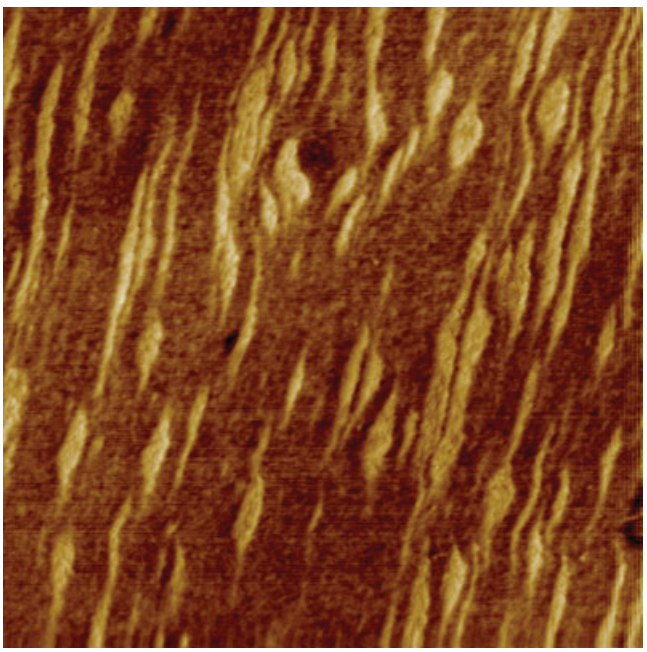

Figure 5 AFM tapping phase micrograph of P-E/PP4292 cast film in MD-ND plane (5 μm by 5 μm). [Color figure can be viewed in the online issue, which is available at www.interscience.wiley.com.]

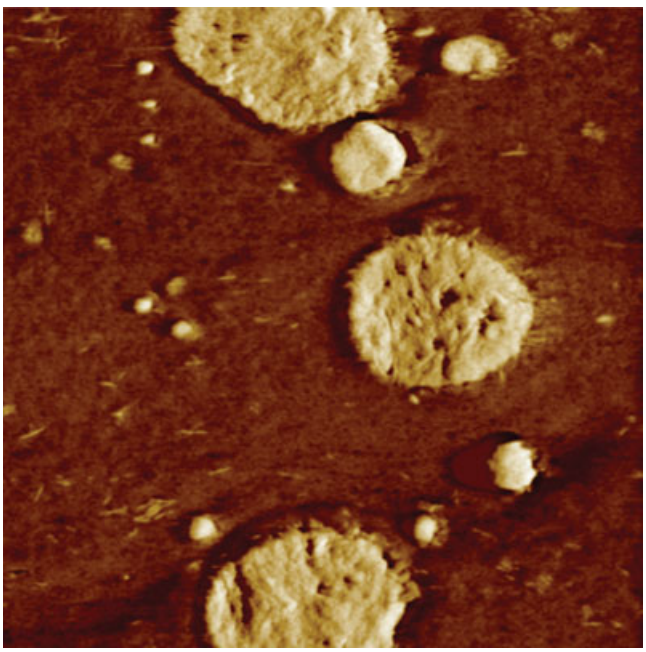

Figure 7 AFM tapping phase micrograph of P-E/HD7755 cast film in MD-ND plane (5 μm by 5 μm). [Color figure can be viewed in the online issue, which is available at www.interscience.wiley.com.]

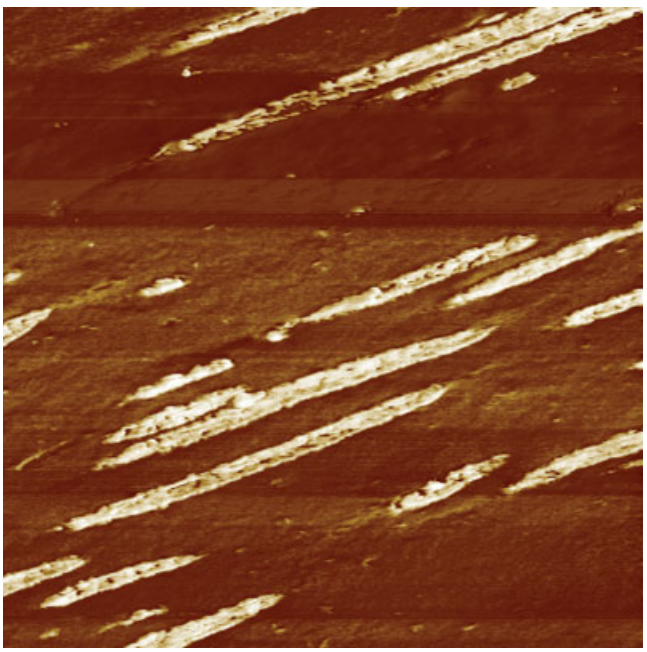

Figure 8 AFM tapping phase micrograph of P-E/HD6705 cast film in MD-ND plane (10 μm by 10 μm). [Color figure can be viewed in the online issue, which is available at www.interscience.wiley.com.]

cated. All equivalent diameter and aspect ratio values are number averages. Shapes and sizes of these dispersions could be rationalized following the Taylor[14,15] theory for Newtonian drop breakup and deformation under planar extensional flow.

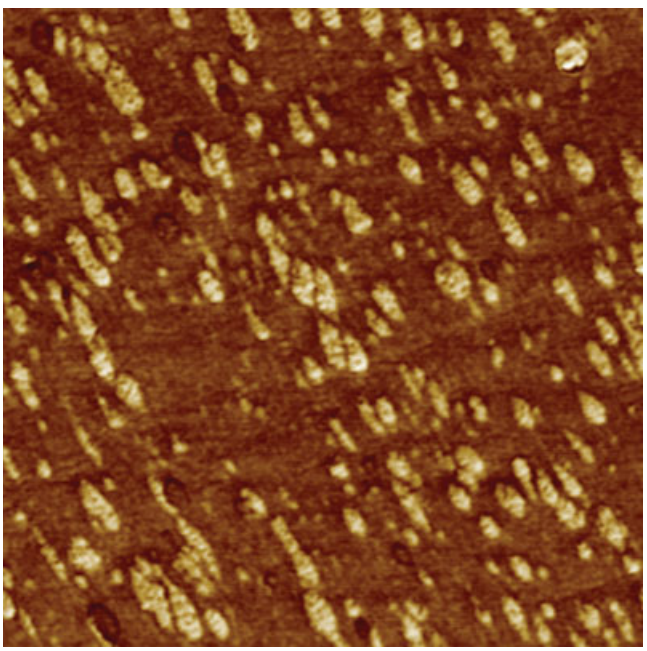

Figure 9 AFM tapping phase micrograph of P-E/PP4292 cast film in TD-ND plane (5 μm by 5 μm). [Color figure can be viewed in the online issue, which is available at www.interscience.wiley.com.]

TABLE V
Equivalent Diameters and Aspect Ratios of Cast Films from P-E Blends

Blend	Plane	Equivalent diameter (μm)	Aspect ratio
P-E/PP4292	MD-ND	0.28	4.5
P-E/PD4443	MD-ND	0.19	7.5
P-E/HD7755	MD-ND	0.67	1.5
P-E/HD6705	MD-ND	0.86	6.5
P-E/PP4292	TD-ND	0.11	2.1
P-E/PD4443	TD-ND	0.08	2.6
P-E/HD7755	TD-ND	0.25	1.5
P-E/HD6705	TD-ND	0.14	1.5

Birefringence in P-E films

Deformation and alignment of these dispersions during film casting will contribute both directly and indirectly to the overall orientation of the final film. PBR and IPR values are reported in Table VI, where it can be seen that both values increase with casting speed. The birefringence values of P-E/PP films are systematically larger than those of P-E/HDPE films. All in-plane orientations are toward machine direction (with a positive IBR value), consistent with the observation of machine-direction alignment of the dispersions. The higher average refractive indices of P-E/HDPE films compared with those of P-E/PP films simply reflect the higher density (or crystallinity) of PE dispersions. Both in-plane and planar birefringence are removed after annealing the P-E/HDPE films, whereas the planar birefringence is only slightly reduced for the P-E/PP films. The ability to remove birefringence in films from P-E blends by annealing at temperatures above the melting point of the P-E matrix, but below the melting point of the dispersed phase, suggests that the birefringence is largely due to orientation of the P-E matrix.

Stress-induced orientation and birefringence from concentrated stresses around rigid fillers in filled polymers under deformation have been observed and modeled.[16] Similarly, concentrated stresses at the tips of ellipsoidal dispersions during casting could lead to orientation and birefringence in the P-E matrix around the dispersions. While the observation of lamellae penetrations at the interfaces of P-E/PP blends suggests strong interfacial couplings between P-E and PP, there are no indications of interfacial coupling at interfaces for P-E/PE blends. Therefore, PP dispersions with strong interfacial adhesion should lock in the orientation more than that of PE dispersions resulting in higher birefringence values in P-E/PP films. Also, because of strong interfacial interactions between PP and P-E prevent P-E chains around the dispersions from relaxing, only slight reductions in orientations are indicated in P-E/PP films after annealing. In contrast, weak interac-

TABLE VI
Birefringence Values of P-E Films

Film	Casting speed (rpm)	Annealing	PBR	IBR	⟨n⟩
P-E	40	No	0.0005[a]	0.0004[a]	1.4811
P-E/PP4292	40	No	0.0038	0.0061	1.4853
P-E/PD4443	40	No	0.0071	0.0013	1.4856
P-E/HD7755	40	No	0.0026	0.0051	1.4912
P-E/HD6705	40	No	0.0021	0.0029	1.4905
P-E/PP4292	80	No	0.009	0.0158	1.4868
P-E/PD4443	80	No	0.0117	0.0212	1.4866
P-E/HD7755	80	No	0.0081	0.0148	1.4923
P-E/HD6705	80	No	0.0029	0.0044	1.4900
P-E/PP4292	40	Yes	0.0040	0.0036	1.5012
P-E/PD4443	40	Yes	0.0063	0.0104	1.4848
P-E/HD7755	40	Yes	N/M[b]	N/M	N/M
P-E/HD6705	40	Yes	0.0002[a]	−0.0005[a]	1.4890

[a] Values are within the sensitivity limit of the instrument.
[b] N/M cannot be measured due to film opaqueness after annealing.

tions between P-E and HDPE allow P-E to relax completely during annealing leading to almost zero birefringence.

Elongation to break of P-E films

All compression molded P-E films have break strains of around 1600% for both neat films and films from blends. Orientation in compression molded pads is negligible. However, as indicated in Figure 10, break strains are reduced significantly by even the slightest degree of orientation introduced by the film casting process (reflected in a twofold drop in elongation to break when going from an isotropic film to a cast film with only 0.0005 birefringence), and continue to decrease with increasing planar orientation. The reason for this severe degradation in elongational properties of P-E associated with a small amount of orientation is not known and warrants further study. Considering that this curve in Figure 10 includes data from films of both neat P-E and P-E blends, it is suggested that the break elongation of a fabricated part based on P-E blends depend mostly on orientation of the P-E matrix. Orientation in films from P-E blends can be suppressed with the benefit of increasing film elongation by either film annealing or blending with HDPE.

Elastic recovery of P-E films

Recovery values of P-E films are expected to be compromised by blending with PP or HDPE because these blend component are plastic in nature. However, as shown in Figure 11, increasing orientation results in further reduction in elastic recovery, although the dependence is weak compared with that for break strain. The data scatter observed in Figure 11 suggests that there are other factors contributing to the elastic recovery of P-E films. According to finite element simulation results of P-E containing a single PP dispersion under an applied strain of 100% (see Figs. 12 and 13), the maximum strain around a spherical PP dispersion was found

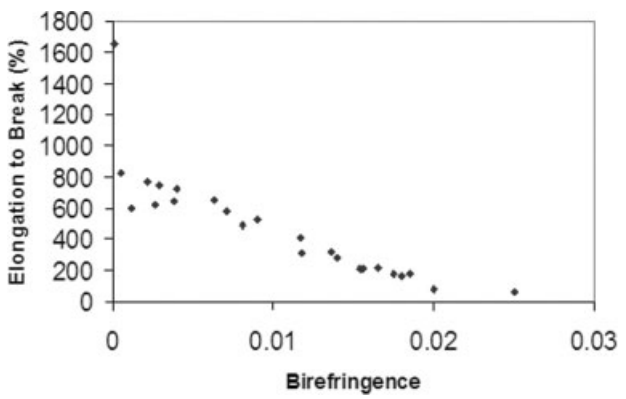

Figure 10 Orientation and break strains in P-E films.

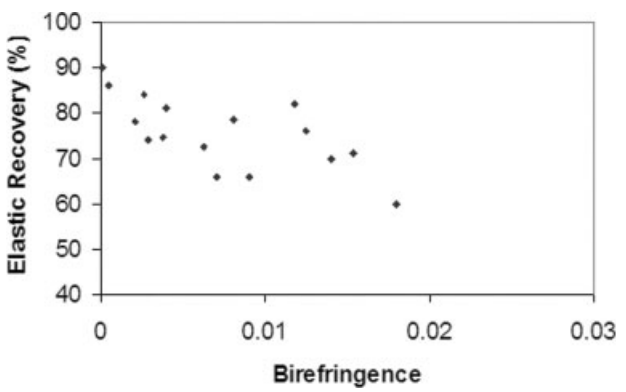

Figure 11 Orientation and elastic recovery values in P-E films.

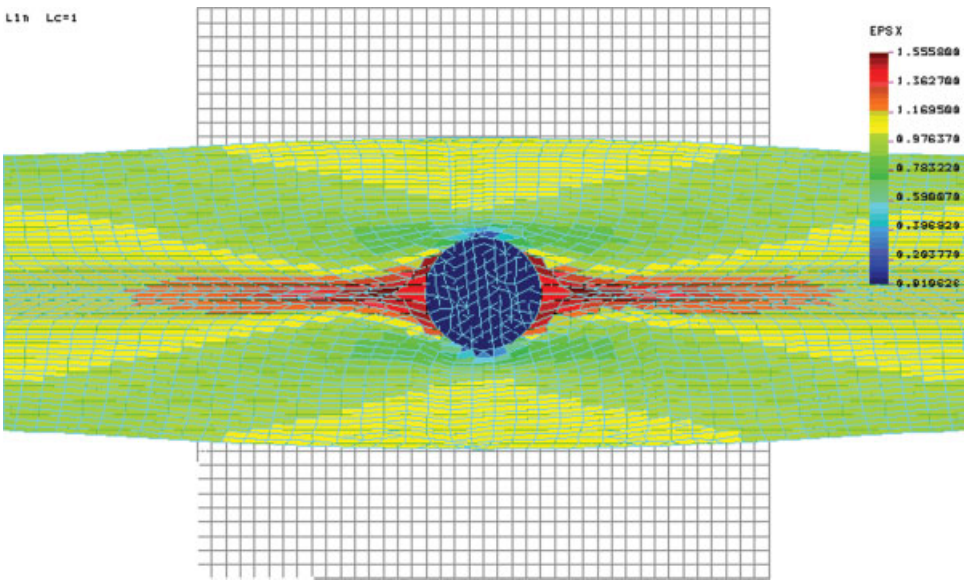

Figure 12 Equivalent strain profile of P-E with a spherical PP dispersion elongated to 100%. [Color figure can be viewed in the online issue, which is available at www.interscience.wiley.com.]

to be 155% whereas the maximum strain at the tip of an elliptical PP dispersion was 353%. Because elastic recovery in P-E decreases with increasing strain, P-E films containing ellipsoidal dispersions aligned in the machine direction can have much higher internal strains at the dispersion tips than the externally applied strains and subsequent lower recovery values.

The reduction in recovery resulting from dispersed PP or HDPE is directly related to the tip radius of the dispersed particles, suggesting that strain amplification is an important factor in understanding the observed low elastic recovery of P-E films containing ellipsoidal dispersions. For an elliptical cavity in a two-dimensional plate under uniform stress, σ, the maximum stress occurs at the ends of the major axis of this elliptical cavity given by the formula of Inglis.[17]

$$\sigma_{max}/\sigma = (1 + 2a/b) \tag{13}$$

Here 2a and 2b are the major and minor axes of the ellipse, respectively. The right hand side of eq. (13) is the stress concentration factor. For a spherical cav-

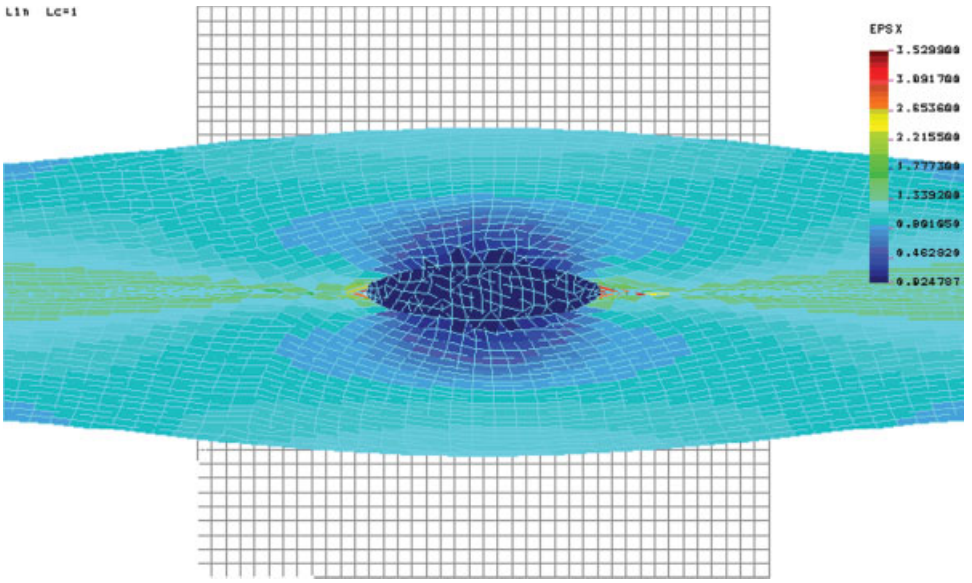

Figure 13 Equivalent strain profile of P-E with an elliptical PP dispersion elongated to 100%. [Color figure can be viewed in the online issue, which is available at www.interscience.wiley.com.]

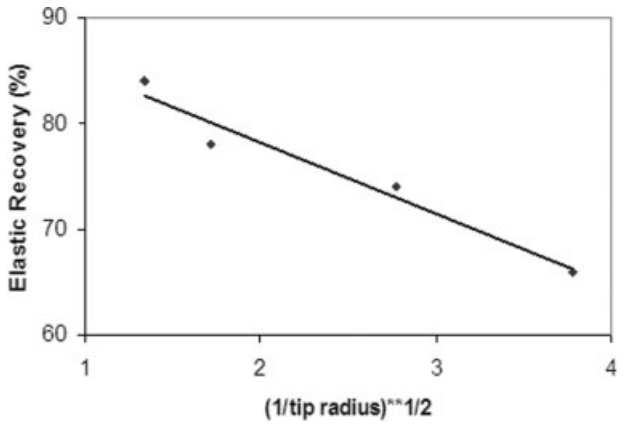

Figure 14 Elastic recovery values and dispersion tip radii of P-E films.

ity, the stress concentration factor is 3. The value of stress at the leading edge of the cavity becomes extremely large as the ellipse is flattened. In the case of an extremely flat ellipse having a radius of curvature $\rho = b^2/a$, eq. (13) can be written as

$$\sigma_{max}/\sigma \sim= 2(a/\rho)^{1/2} \quad (14)$$

The stress concentration factor depends more on form (or shape) of the cavity than on its size. Following eq. (14) for flat ellipses, elastic recovery of P-E films is found to be proportional to the square root of dispersion tip radius in Figure 14. All tip radii were measured in the MD-ND plane as number averages.

CONCLUSIONS

During film casting, the orientation imposed on a propylene–ethylene (P-E) elastomer lowers the extensibility and elastic recovery of films prepared from either neat P-E or P-E blends with ''hard'' plastics like PP or HDPE. In addition, the presence of dispersed phases of PP or HDPE, which are drawn into elongated ellipsoids aligned in the machine direction, further reduces the recovery of these P-E blends. All in-plane orientation is found to be parallel to the machine direction, consistent with the observation of machine-direction alignment of the dispersions. Orientation in P-E/HDPE films is removed after annealing, whereas planar orientation in P-E/PP films is only slightly reduced. The presence of PP domains with strong interfacial adhesion to the matrix could ''lock in'' the orientation more readily than in HDPE dispersions.

A simplified relationship between elongation to break values of P-E films (with or without blending) and their planar orientation has been established. An increase in planar orientation in a P-E film leads to a reduction in its break strain. Using finite element simulation to analyze deformation mechanism in films from P-E blends, reduction in elastic recovery was attributed to strain amplification around the dispersions. This reduction in recovery is directly proportional to the square root of the dispersion tip radius. Ellipsoidal deformation of dispersions in P-E blends could be suppressed with the benefit of minimizing the loss of elastic recovery by using dispersions with high viscosity and interfacial tension, such as HDPE dispersions.

This work would not have been possible without help from Regina Netherly, Amy Nipe, Cheryl Stevens, Tom Sykes, and Margaret Ynostroza. Contributions from Andrew Peacock, Srivatsan Srinivas, and Alan Galuska are greatly acknowledged.

References

1. Toki, S.; Sics, I.; Burger, C.; Fang, D.; Liu, L.; Hsiao, B. S.; Datta, S.; Tsou, A. H. Macromolecules 2006, 39, 3588.
2. Kramer, E. J. Adv Polym Sci 1983, 52, 33.
3. Palierne, J. F. Rheol Acta 1990, 29, 204.
4. Kerner, E. H. Proc. Roy. Soc. London, B 1956, 69, 808.
5. Graebling, D.; Muller, R.; Palierne, J. F. Macromolecules 1993, 26, 320.
6. Graebling, D.; Muller, R.; Palierne, J. F. J Phys IV 1993, 3, 1525.
7. Goldsmith, P. L. Br J Appl Phys 1967, 18, 813.
8. Tamayo, J.; Garcia, R. Langmuir 1996, 12, 4430.
9. Wicksell, S. D. Biometrika 1925, 17, 84.
10. Underwood, E. E. Quantitative Stereology; Addison-Wesley: Reading, MA, 1969.
11. Hilliard, J. E. Trans Metall Soc AIME 1962, 224, 906.
12. Hardaker, S. S.; Moghazy, S.; Cha, C. Y.; Samuels, R. J. J Polym Sci Part A: Polym Chem 1993, 31, 1951.
13. Tamayo, J.; Garcia, R. Appl Phys Lett 1997, 71, 2394.
14. Taylor, G. I. Proc Roy Soc London A 1932, 138, 41.
15. Taylor, G. I. Proc Roy Soc London A 1934, 146, 501.
16. Ong, C.; Yoon, D. Y.; Stein, R. S. J Polym Sci Polym Phys Ed 1974, 12, 1319.
17. Inglis, C. E. Proc Inst Naval Arch 1913, 55, 163.